Available online at www.sciencedirect.com
SCIENCE DIRECT
Journal of Colloid and Interface Science 283 (2005) 513–517
JOURNAL OF Colloid and Interface Science
www.elsevier.com/locate/jcis

Effects of thermal annealing on the structural and optical properties of $Mg_xZn_{1-x}O$ nanocrystals

J.H. Li [a,b], Y.C. Liu [a,b,*], C.L. Shao [b], X.T. Zhang [c], D.Z. Shen [a], Y.M. Lu [a], J.Y. Zhang [a], X.W. Fan [a]

[a] *Key Laboratory of Excited State Process, Chinese Academy of Sciences, Changchun Institute of Optics, Fine Mechanics and Physics, 16-East Nanhu Road, Changchun 130033, People's Republic of China*

[b] *Center for Advanced Optoelectronic Functional Material Research, Northeast Normal University, Changchun 130024, People's Republic of China*

[c] *Chemistry Department, Jilin University, Changchun 130023, People's Republic of China*

Received 16 June 2004; accepted 9 September 2004

Available online 5 November 2004

Abstract

$Mg_xZn_{1-x}O$ ternary alloy nanocrystals with hexagonal wurtzite structures were fabricated by using the sol–gel method. X-ray diffraction patterns, UV–vis absorption spectra, and photoluminescence spectra were used to characterize the structural and optical properties of the nanocrystals. For as-prepared nanocrystals, the band gap increases with increasing Mg content. Weak excitonic emission with strong deep-level emission related to oxygen vacancy and interface defects is observed in the photoluminescence spectra at room temperature. Thermal annealing in oxygen was used to decrease the number of defects and to improve the quality of the nanocrystals. In terms of XRD results, the grain sizes of nanocrystals increase with increasing annealing temperature and the lattice constants of alloy are smaller than those of pure ZnO. The band gap becomes narrower with increasing annealing temperature. For $Mg_xZn_{1-x}O$ nanocrystals ($x = 0.03$–0.15) annealed at temperatures ranging from 500 to 1000 °C, intense near-band-edge (NBE) emissions and weak deep-level (DL) emissions are observed. Consequently, the quality of $Mg_xZn_{1-x}O$ nanocrystals can be improved by thermal annealing.

Keywords: Sol–gel method; $Mg_xZn_{1-x}O$ alloy nanocrystals; Thermal annealing

1. Introduction

Recently, considerable attention has been paid to ZnO material for realizing a room-temperature ultraviolet laser, which was enabled by the wide direct band gap ($E_g = 3.4$ eV) and large exciton binding energy (60 meV) at room temperature [1,2]. Moreover, ZnO-based materials are being applied in various electronic and optical devices such as solar cells, light-emitting devices, optical waveguide, ultraviolet photo detectors [3–5], etc. To obtain high-quality optoelectronic devices, it is essential to construct a heterojunction structure in order to realize double confinement for carriers and photons in optoelectronic devices. The key problem in this endeavor is to find a way to adjust the band gap while keeping the lattice constants similar between the materials constructing the heterojunction [3]. Magnesium oxide (MgO) has a band gap of 7.8 eV and a cubic crystal structure. The ionic radius of Mg^{2+} (0.57 Å) is similar to that of Zn^{2+} (0.6 Å) [3,6], so replacement of Zn by Mg should not cause a significant change in lattice constants. By doping suitable Mg into ZnO, it may be possible to obtain a ternary $Mg_xZn_{1-x}O$ alloy with a wider band gap than pure ZnO, yet still having a lattice constant similar to that of pure ZnO. These properties may enable $Mg_xZn_{1-x}O$ to form heterostructures with ZnO that can be used in UV detectors [4].

At present, many methods have been used to prepare $Mg_xZn_{1-x}O$ alloys, such as pulsed-laser deposition (PLD)

* Corresponding author.
E-mail address: ycliu@nenu.edu.cn (Y.C. Liu).

0021-9797/$ – see front matter
doi:10.1016/j.jcis.2004.09.011

[3,4], radiofrequency magnetron sputtering (RFMS) [5], laser molecular beam epitaxy (L-MBE) [7,8], and plasma-assisted molecular beam epitaxy (P-MBE) [9,10]. Compared with these methods, the sol–gel method is simple, flexible, and economical. Nanocrystal composition can be controlled easily by adjusting the different ion proportions in the solution [6], and it has proven capable of generating $Mg_xZn_{1-x}O$ nanoparticles in the range of 3–5 nm. Here, $Mg_xZn_{1-x}O$ nanoparticles were successfully synthesized by the sol–gel method in absolute ethanol solutions. The films were fabricated on silicon and quartz substrates by spin coating, followed by thermal annealing at temperatures from 500 to 1000 °C.

2. Experiments

Four types of nearly stoichiometric 0.1 M $Mg_xZn_{1-x}O$ colloids were synthesized with $x = 0.03$, 0.05, 0.1, and 0.15. Preparation procedures were similar to those reported in Refs. [11–13]. Here, Zn^{2+} and Mg^{2+} were prepared with zinc acetate ($ZnAc_2{\cdot}2H_2O$) and magnesium acetate ($MgAc_2{\cdot}2H_2O$), respectively. Colloids with different Mg^{2+} contents were made as follows: in each case, 0.1 L of absolute ethanol containing 0.1 M Zn^{2+} and Mg^{2+} was put into a distillation apparatus so that the solution could run the reaction under ambient atmospheric pressure and avoid moisture exposure. The solution was refluxed, with stirring for 3 h. Next, 4.54 ml tetraethylammonium hydroxide ($(CH_3)_4NOH$) was added and the ethanol solution was stirred for 15 min at 0 °C. This procedure accelerated the release of OH^- ions and resulted in an immediate reaction to form a stable $Mg_xZn_{1-x}O$ solution. Acetate was removed by hexane washing, and the resulting $Mg_xZn_{1-x}O$ solutions were spin-coated onto n-type silicon and quartz substrates to form films, which were then annealed at different temperatures from 500 to 1000 °C in oxygen ambient for 1 h to improve nanocrystal quality.

X-ray diffraction was performed on a D/max-rA X-ray diffractometer (Rigaku) using a Cu$K\alpha$ line of 1.5418 Å to determine the crystal structure. Photoluminescence (PL) spectra were measured using a JY UV-lamb Micro-laser Raman spectrometer in a back-scattering geometry configuration. A He–Cd laser with a wavelength of 325 nm was used as the excitation source for PL measurement. Optical absorption spectra were measured using a UV-360 spectrophotometer (Shimadzu).

3. Results and discussion

3.1. Structural and optical properties of as-prepared nanocrystals

Fig. 1 shows the XRD pattern of an as-prepared $Mg_{0.03}Zn_{0.97}O$ nanocrystal. Five peaks with wide full width at half-maximum (FWHM) of (100), (101), (102), (110), and (103) indicate a nonpreferential-orientation wurtzite structure. As is well known, XRD patterns are composed of superposed diffraction patterns of many particles. Therefore, the XRD pattern broadens with decreasing grain size. Mean grain size was calculated via Scherrer's formula,

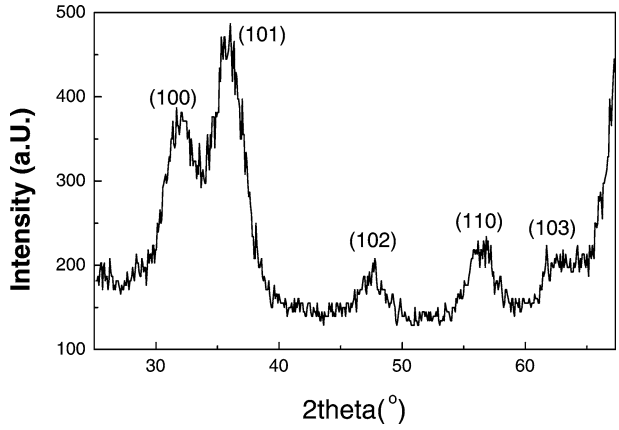

Fig. 1. XRD spectrum of an unannealed $Mg_{0.03}Zn_{0.97}O$ sample.

$$d = \frac{0.9\lambda}{B\cos\theta_B}, \tag{1}$$

where, λ, θ_B, and B are the X-ray wavelength (1.5418 Å), Bragg diffraction angle, and linewidth at half-maximum, respectively. The mean grain size is 5.7 nm bigger than that reported in Ref. [11], as a result of the particle conglomeration process. The lattice constants a and c of the nanocrystal were calculated according to the following equations:

$$a = \frac{\lambda}{2\sin\theta}\sqrt{\frac{4}{3}(h^2+hk+k^2)+\frac{l^2}{(c/a)^2}}, \tag{2}$$

$$c = \frac{\lambda}{2\sin\theta}\sqrt{\frac{4}{3(a/c)^2}(h^2+hk+k^2)+l^2}, \tag{3}$$

where, h, k, l are Miller exponents, and λ and θ are X-ray wavelength ($\lambda = 1.5418$ Å) and Bragg angle, respectively. Here, the resulting values $a = 3.207$ and $c = 5.188$ are smaller than those of pure ZnO ($a = 3.25$, $c = 5.2$) due to Mg atoms entering the ZnO lattice.

The photoluminescence spectra and the UV–vis spectra were measured at room temperature to investigate the optical properties of nanocrystals. Fig. 2 shows PL and absorption spectra of as-prepared samples. The absorption edge shows a clear dependence on the Mg content, x. This result is in good agreement with the report in Ref. [3]. As shown in the inset of Fig. 2, the exciton absorption peak position increases gradually to 4.4 eV for $0.03 \leqslant x \leqslant 0.15$. The absorption edge broadens due to the influence of new $Mg_xZn_{1-x}O$ network with different order degrees. This disorder results from substituting Mg for Zn and increases with increasing Mg concentration. According to Ref. [10], photoluminescence of $Mg_xZn_{1-x}O$ films can be attributed to near-band-edge (NBE) emission and deep-level (DL) emission. Gen-

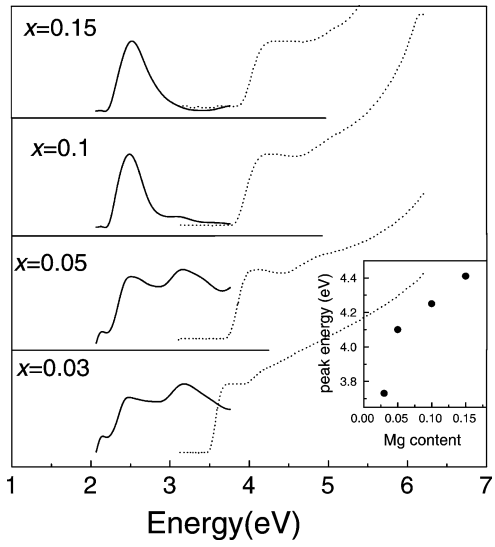

Fig. 2. Photoluminescence (solid lines) and absorption (dotted lines) spectra of $Mg_xZn_{1-x}O$ nanocrystals.

erally, DL emission is considered to relate to the oxygen vacancy and interface defects, while NBE emission is attributed to ultraviolet excitonic emission. For our samples, quantum-confinement effect and bound exciton emission are two dominant factors affecting the NBE peak position. Increasing grain size and bound exciton emission can lead to a red shift in the NBE peak position. In the PL spectra, weak NBE emissions with strong DL emissions are observed. It can be observed that the DL emissions increased compared to the NBE emissions. The NBE emission peak shifts toward lower energy with increasing x. This observation can be explained by the presence of defects introduced into the lattice network by substituting Mg atoms for Zn atoms. Thus, the bound excitons increased with increasing x. As a result, the NBE emission shifts to the low energy side.

3.2. Thermal annealing effect on annealed samples

Thermal annealing in oxygen is an effective method for reducing defects and improving nanocrystal quality. Samples with different x were annealed at different temperatures from 500 to 1000 °C. The XRD pattern in Fig. 3 shows that $Mg_{0.15}Zn_{0.85}O$ film possesses a polycrystalline hexagonal wurtzite structure. It can be seen that the diffraction peak positions of the alloy nanocrystals have a slight shift from the $Mg_{0.03}Zn_{0.97}O$ peak position. This is from the change of the lattice constants of MgZnO alloy. The XRD linewidths become narrower with increasing annealing temperature, indicating progressively enhanced crystallinity increasing mean grain size. Table 1 shows calculated values for the mean grain size (S) and lattice constants a (L_a) and c (L_c) for the samples with $x = 0.15$, where annealing temperature (T_a) ranges from 500 to 1000 °C. The particles have gradually conglomerated to big clusters. The FWHM of diffraction peaks is observed becoming narrower than that of

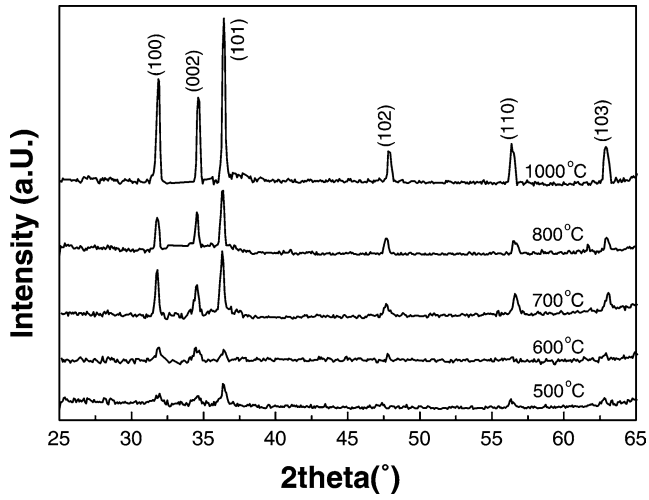

Fig. 3. The XRD spectra of $Mg_{0.15}Zn_{0.85}O$ nanocrystals annealed at different temperatures from 500 to 1000 °C.

Table 1
Lattice constants versus annealing temperature

T_a (°C)	500	600	700	800	1000
L_a (Å)	3.235	3.25	3.242	3.252	3.245
L_c (Å)	5.177	5.193	5.205	5.198	5.18
S (nm)	17.6	19.2	22.9	23.4	24.2

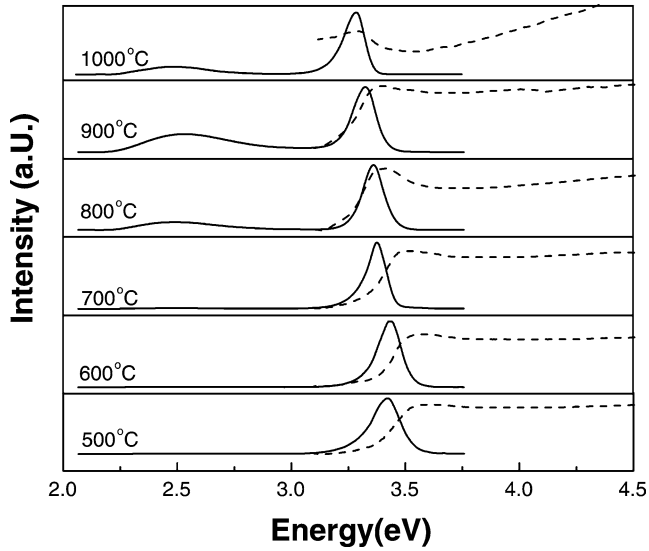

Fig. 4. Photoluminescence (solid lines) and absorption (dotted lines) spectra of $Mg_{0.15}Zn_{0.85}O$ nanocrystals.

unannealed samples, which indicates the improving crystal quality.

Fig. 4 shows room-temperature PL and absorption spectra of $Mg_{0.15}Zn_{0.85}O$ films annealed at 500 to 1000 °C. With increasing annealing temperature, red-shifted intense excitonic absorption and NBE emission with only weak DL emission are observed, verifying the advantageous effects of thermal annealing on adjusting the optical properties of the nanocrystals. The ratio of NBE intensity to DL intensity is an

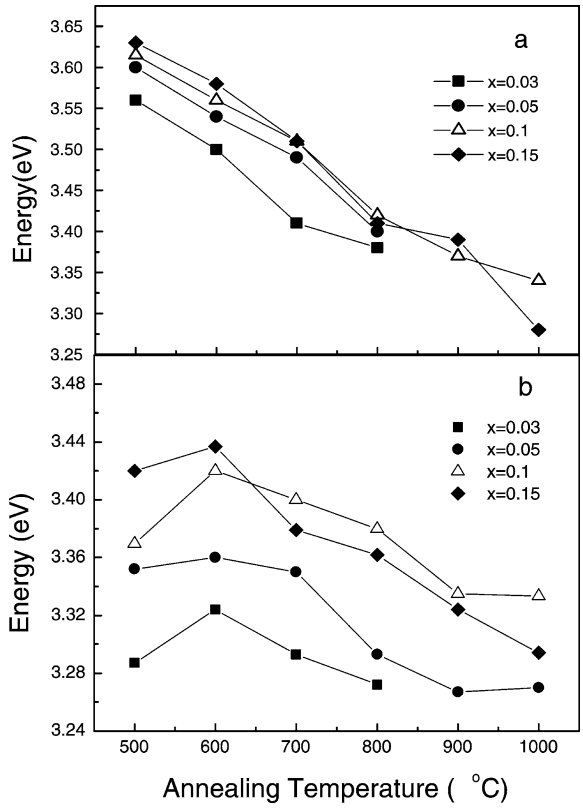

Fig. 5. (a) The UV–vis absorption peak position as a function of annealing temperature; (b) the photoluminescence peak position as a function of annealing temperature.

effective measure of MgZnO crystal quality. From the data in Fig. 4, calculated PL intensity ratios I_{NBE}/I_{DLE} ($PLIR_{ND}$) of $Mg_{0.15}Zn_{0.85}O$ films at different annealing temperatures were 26.9, 71.8, 27.2, 2.8, 1.1, and 3.3, corresponding to 500, 600, 700, 800, 900, and 1000 °C, respectively. The largest value of R_{ND} that indicates the best crystal quality at 600 °C. The peak energies of PL are consistently located on the lower energy side of those of absorption peaks. From 500 to 600 °C, rapidly decreasing defects result in the slight blue shift of the PL peak. At 700 °C, the PL peak continues shifting to the lower energy side with increasing annealing temperature. It is possible that new defects, such as oxygen vacancies and Zn interstitials, may regenerate in the films at higher annealing temperatures, leading to a red shift and decrease of NBE emissions. Furthermore, increasing mean grain size is also a primary contributor to the red shift of NBE emission and absorption peak. In Fig. 4, the slope of the absorption edge does not change noticeably. Compared to Fig. 2, it can be concluded that Mg concentration, rather than annealing, affects significantly the slope of the absorption edge.

Fig. 5a shows the annealing-temperature dependence of the absorption peak energy. The absorption peak energy decreases linearly with increasing annealing temperature for $0.03 \leqslant x \leqslant 0.05$. This decrease can be primarily attributed to increasing grain size with increasing annealing temperature. Fig. 5b shows the annealing-temperature dependence of the PL peak energy. For each value of x, the PL peak energy is maximum at 600 °C, indicating that thermal annealing decreases the defects in the films and improves the crystal quality. From 700 to 1000 °C, the PL peak energy decreases with increasing mean grain size.

4. Conclusions

In conclusion, $Mg_xZn_{1-x}O$ nanocrystals were fabricated by the sol–gel method. The effect of thermal annealing in ambient oxygen on optical and structural properties was investigated by absorption spectra, photoluminescence spectra, and X-ray diffraction patterns. Bound exciton emission and quantum-confinement effects are the two dominant factors affecting optical properties of these nanocrystals. The optical band gap and photoluminescence peak can be tuned to the high-energy side, maintaining high crystallinity without a significant change of the lattice constant, compared to pure ZnO. Strong ultraviolet excitonic emission and weak deep-level emission indicate that thermal annealing in ambient oxygen reduced film defects and improved the nanocrystal quality.

Acknowledgments

This work was supported by the Program of CAS Hundred Talents, the National Fundamental Applied Research Project, the Key Project of the National Natural Science Foundation of China No. 69896260, and the National Natural Science Foundation of China Nos. 60376009 and 60278031.

References

[1] A. Ohtomo, M. Kawasaki, I. Ohkubo, H. Koinuma, T. Yasuda, Y. Segawa, Appl. Phys. Lett. 75 (1999) 980–982.
[2] H.D. Sun, T. Makino, N.T. Tuan, Y. Segawa, Z.K. Tang, G.K.L. Wong, M. Kawasaki, A. Ohtomo, K. Tamura, H. Koinuma, Appl. Phys. Lett. 77 (2000) 4250–4252.
[3] A. Ohtomo, M. Kawasaki, T. Koida, K. Masubuchi, H. Koinuma, Y. Sakurai, Y. Yoshida, T. Yasuda, Y. Segawa, Appl. Phys. Lett. 72 (1998) 2466–2468.
[4] W. Yang, R.D. Vispute, S. Choopun, R.P. Sharma, T. Venkatesan, H. Shen, Appl. Phys. Lett. 78 (2001) 2787–2789.
[5] T. Minemoto, T. Negami, S. Nishiwaki, H. Takakura, Y. Hamakawa, Thin Solid Films 372 (2000) 173–176.
[6] D.X. Zhao, Y.C. Liu, D.Z. Shen, Y.M. Lu, J.Y. Zhang, X.W. Fan, J. Cryst. Growth 234 (2002) 427–430.
[7] J.W. Tomm, B. Ullrich, C.G. Qiu, Y. Segawa, A. Ohtomo, M. Kawasaki, H. Koinuma, J. Appl. Phys. 87 (2000) 1844–1846.
[8] T. Maakino, G. Isoya, Y. Segawa, C.H. Chia, T. Yasuda, M. Kawasaki, A. Ohtomo, K. Tamura, H. Koinuma, J. Cryst. Growth 214–215 (2000) 289–293.
[9] Y.F. Chen, H.J. Ko, S.K. Hong, T. Yao, Appl. Phys. Lett. 76 (2000) 559–562.

[10] D.M. Bagnall, Y.F. Chen, Z. Zhu, T. Goto, T. Yao, J. Cryst. Growth 184–185 (1998) 605–609.
[11] L. Spanhel, M.A. Anderson, J. Am. Chem. Soc. 113 (1991) 2826.
[12] X.T. Zhang, J.Q. Zhuang, Y.L. Ren, J.J. Xu, D.J. Wang, Y.B. Bai, T.J. Li, J.N. Yao, Chinese J. Phys. Chem. 16 (2000) 636.
[13] M. Hilgendorff, L. Spanhel, Ch. Rothemausler, G. Muller, J. Electrochem. Soc. 145 (1998) 3632.